FAÇADE DESIGN EFFECT ON CROSS-VENTILATION IN TAIWANESE SCHOOL BUILDINGS

W.H. Chiang, H.H. Hsu,[a] and J.S. Huang

ABSTRACT

This study performed a three-dimensional numerical prediction for the induced airflow patterns and mean age of air (MAGE) around and inside a naturally ventilated school building, while accounting for the wind profile effect. Various fenestrations, hallways, and shading devices on the windward side of building were analyzed to determine how they affected wind velocity, the incident angle of airflow, and MAGE distribution inside classrooms. The numerical scheme is based on a commercial computational fluid dynamics (CFD) code, PHOENICS. The incline of incoming wind was observed on higher floors that decreased the air exchange rate in the simulated room. The inclined airflow could be effectively deflected downward through the breathing zone by hallways, 1.2-m shades as overhangs, and 0.6-m louvers. Based on this research, an appropriate combination of external attachments on the windward side of building façade can be utilized to enhance ventilation in school buildings. (See Appendix 1 for nomenclature.)

KEYWORDS

cross ventilation, wind profile effect, shading devices, mean air age, computational fluid dynamics (CFD)

1. INTRODUCTION

Elementary and high school buildings in Taiwan, unlike college or university buildings, rely heavily on natural ventilation to remove heat and contaminants. In addition, the ample open space, greenery, and large trees contribute to cooling the outdoor air and increasing wind velocity. Passive cooling by natural wind becomes an attractive means in days with the ever-increasing consumption of energy, especially in the hot and humid climate in Taiwan. Effective ventilation efficiency corresponds to positive effects on indoor air movement, thereby, providing an appropriate airflow velocity for maintaining thermal comfort.

2. LITERATURE REVIEW

2.1 Cross-Ventilation

Natural ventilation is induced by temperature and pressure differences between the inlet and outlet openings of a building, resulting in stack-ventilation and cross-ventilation, respectively.

[a]Corresponding author: H.H. Hsu, Ph.D. Candidate, Tel.: +886-931338860, Fax: +886-2-27376721, E-mail: ashine.hsu@gmail.com (mainly), faye0421@msn.com. Department of Architecture, National Taiwan University of Science and Technology, Taiwan.

Cross-ventilation can be more favorable for providing larger air flow rates and is, hence, more suitable for large heat gains [1, 2]. It is characterized by the presence of two or more openings on opposite sides of a building. Positive pressure is created on the side of the building that faces the wind (windward side); whereas suction regions are formed on the other sides, particularly the opposite side (leeward side).

The external wind field effect and internal airflow structure both determine the geometrical and physical parameters that govern the accuracy of macroscopic airflow when predicting cross-ventilation in buildings. Wind field parameters include wind direction, wind velocity, and turbulence fluctuation. Influential factors of internal airflow structure include building façade configurations such as structural attachments, façade porosity of fenestration, and interior divisions.

2.2 Interaction of External and Internal Wind Fields

Some previous studies have considered internal airflow conditions and external wind field effect separately. However, the interaction between buildings and the external environment was revealed to affect human comfort inside buildings [3]. Kato et al. [4] indicated that the airflow rate of cross-ventilation depends on both drag characteristics of internal flow and the total pressure difference between the windward and leeward openings of a building. A primary force produced in internal airflow for a naturally ventilated structure is the external wind pressure. Many previous studies have claimed that indoor and outdoor airflow must be jointly discussed. Straaten [5], Vickery and Karakatsanis [6], Graca et al. [7], and Seifert et al. [8] have found that the internal flow rates were predicted with inexact external pressure distribution values derived using a solid model. The suggested compact integration method proposed by Zhai et al. [9] showed directional velocity vectors entering and exiting windows, thus describing the real situation more accurately. The directionality of the velocity vectors also created additional vortices and recirculation zones inside a room. Hence, developing scenarios for integrating internal and external wind environment is sufficient for evaluating indoor airflow velocity.

2.3 Wind Profile

The external wind field effect around buildings causes the driving force for cross-ventilation. It is a complex problem involving severe pressure gradients, streamline curvature, swirl, as well as separation and reattachment combined with turbulence effect [10]. External wind field was generally set as average velocity from the previous published papers. However, Straaten's [5] experiment showed that the atmospheric boundary layer effect appeared when the mean wind velocity increased with height as a consequence of friction between the layer of moving air and the ground. The roughness of the terrain apparently influenced the gustiness of the wind and variability of its direction. Accordingly, assuming the wind profile inlet is necessary in designing the studied domain.

2.4 Building Façade Design

Building façade configurations determine the wind airflow direction that enters a building, and profoundly affects the microclimate of a building [10, 11]. Ayad [10] studied the ventilation properties of a room with various fenestrations. The results showed that the placement of openings in relation to one another may enhance the mean velocity inside a room. Prianto and Depecker [12] focused on the applicability of some architectural design elements, such as window location, balcony configuration, and interior division, using numerical simulation.

The analysis showed that building façade configuration played a significant role in improving the indoor thermal environment. Chiang et al. [13] and Argiriou et al. [14] discussed the effects of façade design on natural-ventilation and concluded that shading position is the main factor determining airflow velocity in a room.

2.5 CFD Application

Computational fluid dynamics (CFD) has progressed rapidly during the past years in evaluating the interaction between wind and building structures. The applications are extended to examine indoor air quality, as well as natural and stratified ventilation [15]. Studies on the wind field effect using CFD can be mainly divided into several categories, including wind climate predictions of city blocks [16–18] and around buildings [19, 20], mesoclimatic predictions of a room [21, 22], microclimatic predictions around human bodies [23, 24], and predictions integrating all aforementioned categories. Numerous previous studies have proved that predicting airflow patterns and surface pressure distributions using CFD simulations agree favorably with experimental data derived from wind tunnels [25, 26].

3. RESEARCH OBJECTIVES AND PROCEDURE

3.1 Research Objectives

Appropriate ventilation facilitates human comfort in indoor environments. To enhance the efficiency of natural ventilation, wind must be properly channelled through the building. The ventilation rate for a room depends not only on wind field characteristics but also on building façade design. This study developed a full-scale numerical simulation of the wind profile effect to investigate the airflow pattern, velocity, and mean age of air in a room that is influenced by fenestrations of and attachments on the building façade.

3.2 Research Procedure

Cross-ventilation mechanisms have always been implemented in elementary school buildings in Taiwan. This study referred to the sizes of the openings and prototypical classroom plans surveyed by Architecture and Building Research Institute for elementary school classrooms in Taiwan [26]. Fig.1 (a) displays a prototypical classroom. Horizontal sliding windows are commonly used in Taiwan. The dimensions of an individual operable window set are 1.8 m × 1.2 m. The opening areas of the inlet and outlet are designed to be the same and fully opened, which is approximately 12.5% of the façade area. This generally provides the maximal cross-ventilation rate.

Because of large variability, the simulations were conducted with a sequence of settings, as shown in Fig. 2. The examined factors included opening position and larger scale components near the openings such as hallways and shading devices on the windward side.

The first set of simulations was performed to determine optimal fenestration using a simplified four-story building model with a prototypical classroom (Fig. 1 (b)). Fig. 3 shows the four designed layouts for the inlet and outlet opening in our study. There were totally 16 fenestration arrangement combinations. The second set of simulations was performed by extending the simplified model to a complete model by locating five aligned classrooms on each floor, thus representing a typical school building in Taiwan.

The third set of simulations involved using a complete model (Fig. 1 (c)) to determine the effect of adding a 3-m wide hallway on the windward side as shown in Fig. 4 (a). The hallway was expected to reduce the difference in airflow pattern and ventilation efficiency among the floors.

FIGURE 1. (a)–(c) Simulated models.

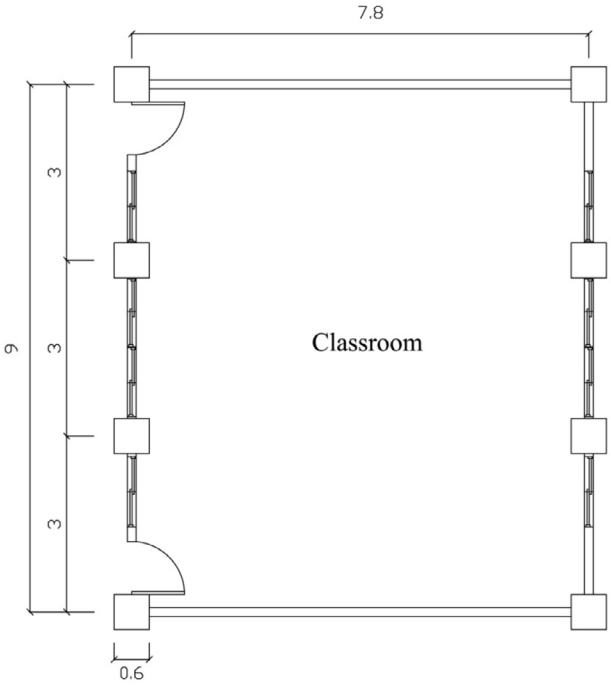

(a) The drawings with dimension for a prototype classroom (unit: m)

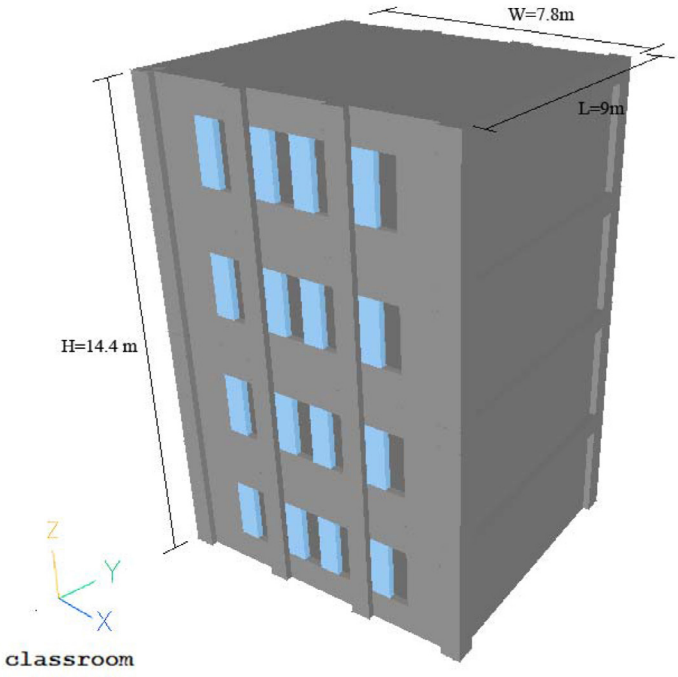

(b) The simplified model with only one classroom on each floor

FIGURE 1. (a)–(c) *(continued)*

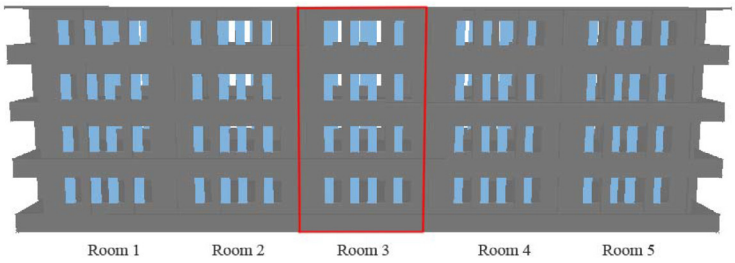

(c) The complete model with five classrooms on each floor

FIGURE 2. The flow chart of research procedure.

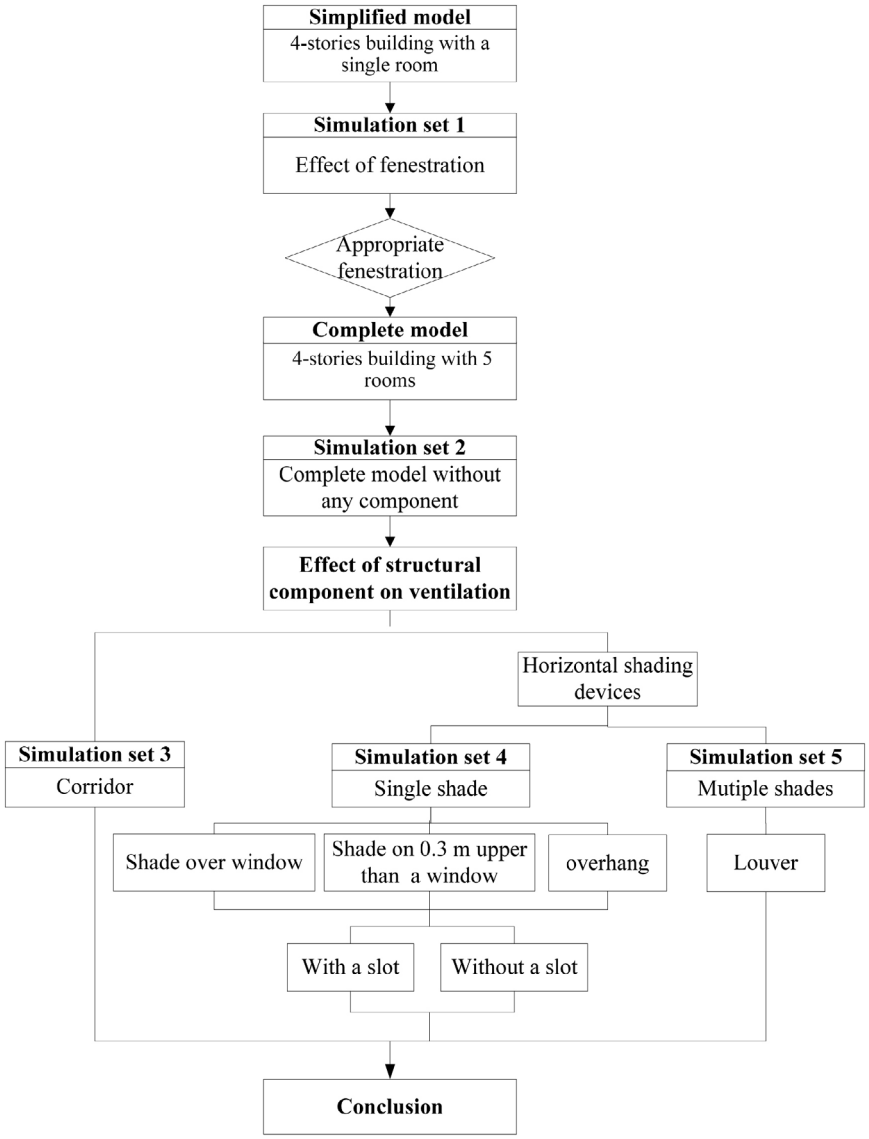

FIGURE 3. (a)–(d) The layouts of opening used for simulation set 1.

(a) A layout (b) B layout

(c) C layout (d) D layout

FIGURE 4. (a)–(e) Dimension of structural attachments on building façade (unit:m).

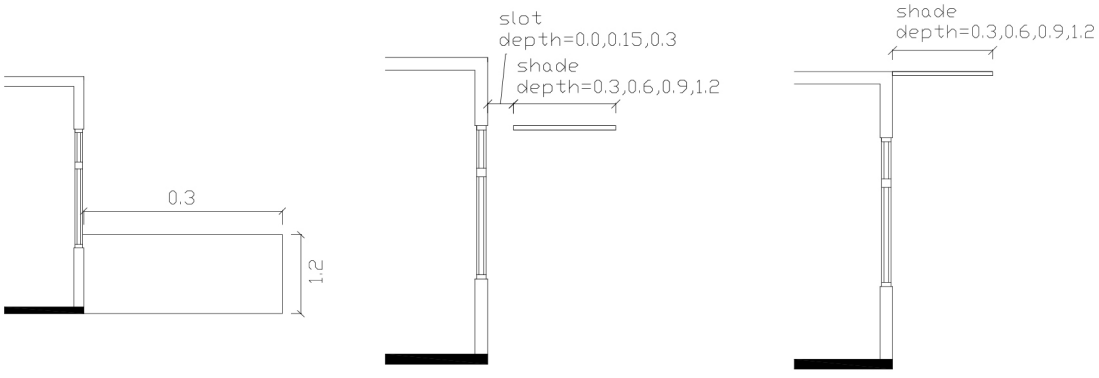

(a) Hallway (b) Horizontal shading (c) Overhangs

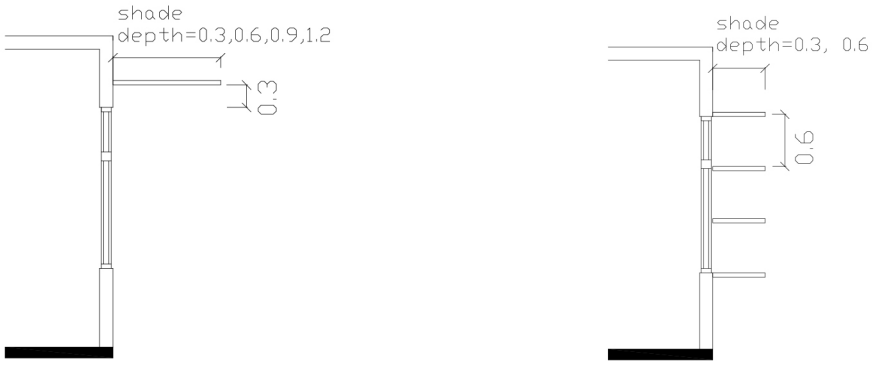

(d) Horizontal shading located on 0.3 upper than a window

(e) Louver

The selected shading devices in this study were focused on horizontal shadings, either in single shade or in multiple shades as a louver. The fourth set of simulations emphasized the single horizontal shadings. The difference between horizontal shading and overhangs depended on its position. The former was near the top of the window, whereas the latter was extended from the ceiling or roof, normally much higher than the top of the window. Therefore, various positions of the shades heights regarding the openings were examined. The shades were either placed on the top of the window, overhang as an extension of the floor, or between the two positions. The precise dimensions and locations of shading devices in each situation are displayed in Fig. 4. However, the external pressures could be equalized using a slot on the horizontal shadings that weakened the upward airflow [28]. Hence, 0.15-m and 0.3-m depth slots on the horizontal shades were also tested as additional research variables in this simulation set.

In the fifth set of simulations, 0.3-m and 0.6-m multiple shades as louver were attached to the façade of the complete model building. Louver devices of 0.9-m and 1.2-m are not discussed because of the inefficiency of indoor lighting. Because the opening area adequately large to achieve satisfactory air quality by measuring air change rate per hour (ACH), this research emphasized airflow velocity distributions and MAGE in the student's breathing zone (1.05 m) in the examined room at the center of complete building.

3.3 Air Quality Index

3.3.1 Air Exchange Rate

The air exchange rate is a general index for evaluating building ventilation and has units of 1/time. When the time unit is hours, the air exchange rate is called air changes per hour (ACH) and can be obtained using Eq. (1) [29]:

$$n = \frac{Q}{V} \tag{1}$$

n (1/hr): air changes per hour

Q (m^3/hr): volumetric flow rate of air into space

V (m^3): interior volume of space

Normally, air exchange rates ranging from 4 to 12 ACH are considered sufficient to remove indoor containments from school buildings [30]. Air exchange rates with much greater values can extract accumulated heat and improve thermal comfort.

3.3.2 Mean Age of Air (MAGE)

The air exchange rate describes the outside air ventilation rate entering a building or zone. However, it does not describe recirculation or the distribution of the ventilation air to each space within a building or zone [31]. Mean age of air, which is defined as the average time for air to travel from the opening to any location inside a ventilated room, can be use to evaluate ventilation efficiency [32]. The concept of MAGE is assumed as zero at the inlet opening (100% fresh) [33]. The "youngest" air is at the point near the window where air enters the room by forced or natural ventilation. The "oldest" air is at a certain location inside the room or in the exhausted air. In "dead" zones (the recirculation areas), the time since entry tend to a large value as the air trapped there [34]. The mean internal age of air () involve units of time that are usually in seconds, and can be obtained using the following transport equation:[35]

$$u_i \frac{\partial_{\bar{\tau}}}{\partial_x} = \frac{\partial}{\partial_{x_i}} \left[\left(\frac{\upsilon_t}{\sigma_{\bar{\tau}}} + \frac{\upsilon}{\sigma} \right) \frac{\partial_{\bar{\tau}}}{\partial_{x_i}} \right] + 1 \quad (2)$$

Where u_i is the velocity component; υ and υ_t are the laminar and turbulent kinematic viscosities, respectively. σ is the laminar Schmidt number of air and $\sigma_{\bar{\tau}}$ is the turbulent Schmidt number for the age of the air. The further formulations may refer to references [34, 36]. In this study, the values were calculated directly from the CFD code PHONEICS.

3.4 CFD Modeling

3.4.1 Computational Domain Size

To examine the effect of wind profile on different height, the simplified model was set as a four-story building, as shown in Fig. 1 (b). The terrain condition for computational domain was assumed as the urban region. The factors of the external surroundings on the flow and dispersion within the computational domain were accounted for with the prescription of the behavior of the flow variables at the boundaries. The airflow entered from the boundaries through the computational domain with complete information on all flow variables was necessary. The COST Action 732 [37] was the guideline for superior model validation of simulations. For a single building model, the top of the computational domain should be at least 5 H above the roof of the building, where H is the building height. The requirement of lateral extension required a distance of 2.3 H between the building's sidewalls and the lateral boundary. At least 5 H between the inflow boundary and the building façade was optimal for the wind profile to be well defined. The extended region behind a single building should be positioned at least 15 H for flow re-development occurring behind the wake region. Based on this assumption, the computational domain dimension in this study was set as 111.44 m in x-axis, 296 m in y-axis, and 86.4 m in z-axis. The wind field greatly influenced the airflow on the building's windward side, forming upstream turbulence that considerably affected the external flow reattachment and surface pressure coefficients. This, in turn, affected airflow through the building openings; and ultimately, the MAGE distribution in the room. The simulations showed that the penetration flow entered the inlet opening with steep inclined angles caused by the front eddy; and the flow exited from the outlet moving upward because of the outside re-circulating eddy. The entire simulated model of the computational domain is displayed in Fig. 5 (a).

3.4.2 Numerical Scheme

The standard *k-ε* turbulence model has been widely used in numerous previous studies. However, Chen [38, 39] studied various indoor airflows using eight turbulence models and concluded that the RNG *k-ε* model demonstrated superior feasibility to predict the indoor airflow velocity. The simulations by Evola and Popov [19] and Posner et al. [20] showed favorable agreement with experiment data, especially when using RNG *k-ε* model. The three-dimensional CFD model with the RNG *k-ε* turbulence developed by Kim and Baik [16] also showed the same result for ambient airflow in urban area. Accordingly, the RNG *k-ε* model is intended to be a useful tool for studying wind-driven natural ventilation, while predicting the assessment of the ventilation rate and air distribution inside a room.

This study used a commercial CFD code, PHOENICS, to solve pressure, velocity, turbulence and MAGE in steady state condition. For the RNG *k-ε* turbulence equation, the empirical turbulence coefficients were set as: $\sigma_\varkappa = 0.7179$, $\sigma_\varepsilon = 0.7179$, $\sigma_{\varepsilon 2} = 1.68$, and $C\mu = 0.085$ [44]. For the MAGE equation, the initial value at the air inlet was zero. Thermal effect was ignored because wind force used in this study was strong than buoyancy effect.

FIGURE 5. (a)–(c) Computational domain and grid settings.

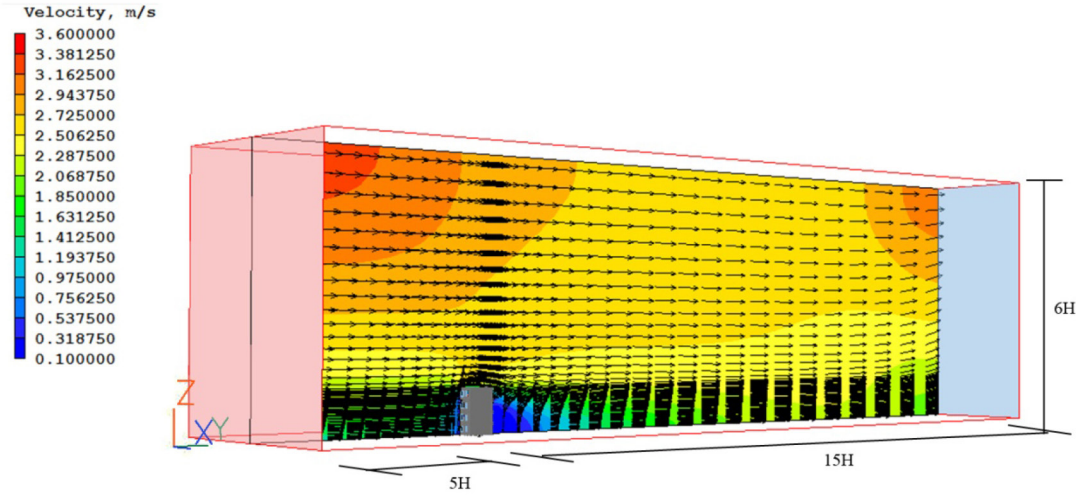

(a) Computational domain

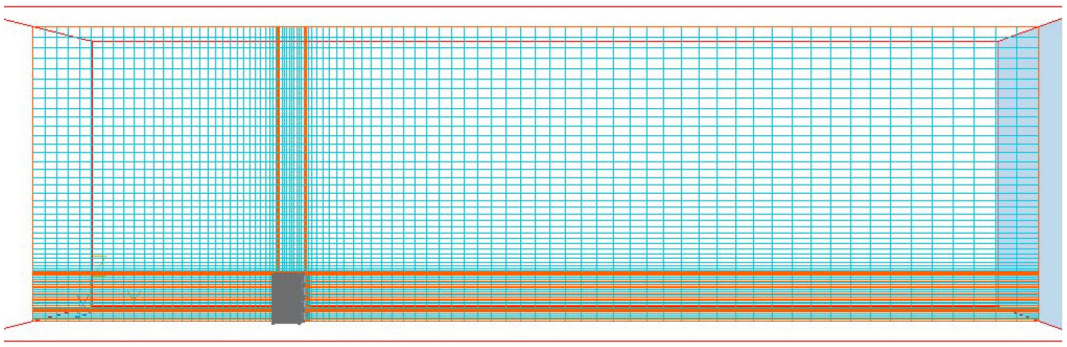

(b) The chosen grid

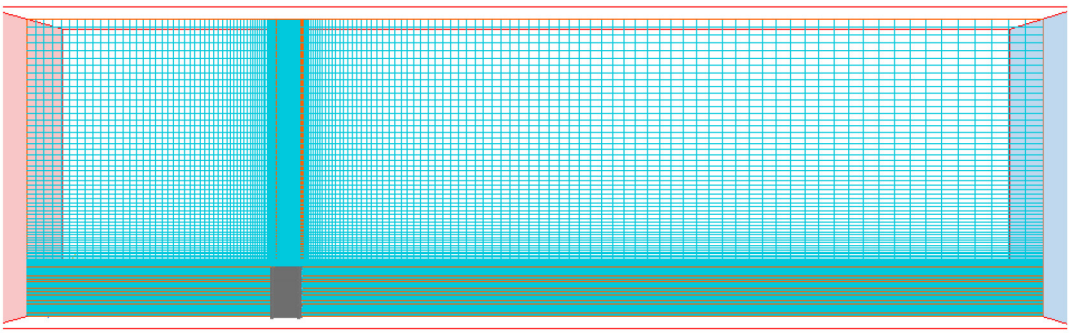

(c) The finer grid

TABLE 1. Summary of cell size used. (Unit: m)

Area	Cell size of chosen grid	Cell size of finer grid
Internal zone*	0.15~1.5	0.0375~0.375
Distance from building in 2 H	0.8~3.0	0.2~1.5
Distance from building over 2 H	3.0~6.0	1.5~3.0

*Areas included the building and attached components of building facade.

To obtain more highly detailed information around and inside the simulated room, the grid used for this study was not uniform in size, and its density was more crowded as more close to the room with the growth rate as 1.2. The non-uniform cell sizes were approximately 0.15 m to 0.8 m for internal zone, including the building and shading devices on the building façade, and 0.8 m to 6 m for external zone (Table 1). The total mesh number is 4,116,000. The iteration of calculation was employed by 25000 to converge achieving the predetermined criteria of 10^{-5}. This study employed CFD to solve the equations by discretizing them using finite volume techniques that convert the flow-governing equations to a set of numerically solvable algebraic equations.

3.4.3 Wind Profile Function

The wind velocity near ground is highly variable and irregular. Such random behavior is designated by the term "turbulence" [40]. In the low atmospheric layers, turbulence is generated by any ground obstacles as well as by thermal airflow instabilities. Turbulence decreases with increasing height. In this study, the inlet boundary conditions associated with a wind velocity profile (considering the atmospheric boundary layer) can be defined using a wind profile function built in the software program PHOENICS. Either a logarithmic or power-law velocity profile can be specified, as follows [41,42]:

Logarithmic profile:

$$\frac{U}{U^*} = \frac{ln}{\kappa}\left(\frac{Z}{Z_o}\right) \tag{3}$$

Power-low profile:

$$\frac{U}{U_r} = \left(\frac{Z}{Z_r}\right)^{\alpha} \tag{4}$$

where U is the total velocity at the height Z from the ground, κ is von Karman's constant (=0.41), and Z_o is the effective roughness height of the ground terrain, U_r is the reference velocity at the reference height Z_r, and α is the power-law exponent.

The wind profile as inlet profile is usually obtained from logarithmic profile [37, 43, 44]. For logarithmic profile formulation of boundary condition, the same coefficients that were used in the turbulence model including the turbulence kinetic energy, k, and its dissipation rate , ε, were used as following :[43–45]

$$k = \frac{U^{*2}}{\sqrt{C_\mu}} \tag{5}$$

$$\varepsilon = \frac{U^{*3}}{\kappa z} \tag{6}$$

The total friction velocity, U^*, is given as :

$$U^* = U_r \frac{\kappa}{ln}\left(\frac{Z_r}{Z_o}\right) \tag{7}$$

The reference height Z_r is usually adopted as 10 m, because this is the height where mean meteorological wind speed data are generally provided. In this study, the velocity at reference height was set as 2 m/s according to the climate statistics over last ten years in Taiwan. The effective roughness height of the ground terrain was 1 m to represent terrain type of urban.

4. RESULT AND DISCUSSION

4.1 Grid-Sensitivity Analysis

To reduce numerical errors, not only iterative convergence but also grid setting should be assessed. In this study, a grid-sensitivity analysis was performed for the simplified model by comparing the chosen grid to a grid with 4 times finer mesh density (Fig.5 (b)–(c)). The exact mesh sizes were listed in table 1. Indoor air velocity as a function of height at the inlet of building centre was evaluated. The chosen grid was considered satisfactory because the maximum discrepancy between the two grids was 10% (Fig.6).

4.2 CFD Validation

To ensure the validity of numerical procedure and boundary condition for this study, an additional set of simulations was conducted that replicated the experiments by Givoni [40, 46–52]. A room with two windows on opposite walls was used where the inlet directly faced the external wind. Average indoor air velocity, expressed as the percentage of external wind

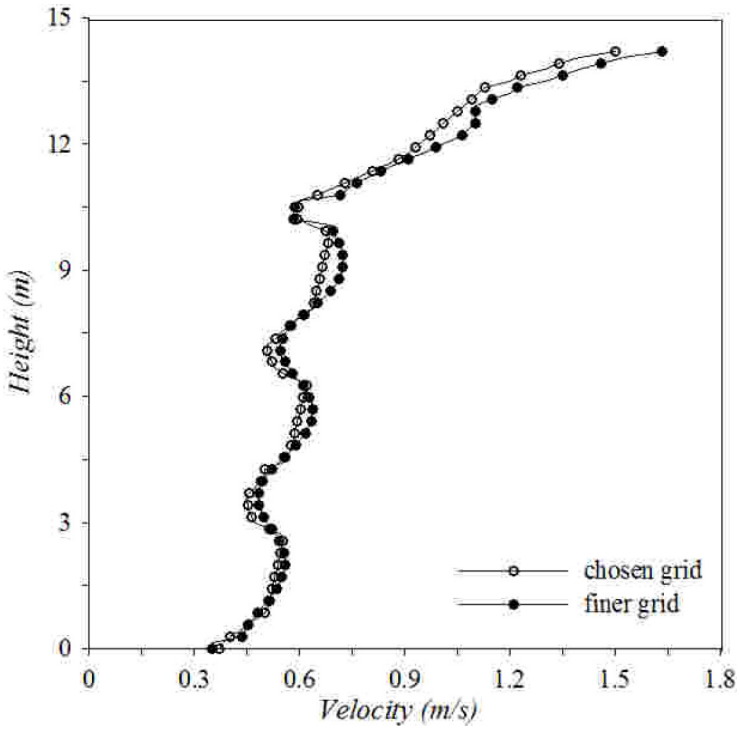

FIGURE 6. Wind velocity as a function of height at the inlet of building centre comparing the chosen grid to the finer grid.

TABLE 2. Average indoor air velocity as the percentage of external wind speed comparing simulated data with published experimental data. (unit: %)

Inlet Width	Outlet Width	Givoni's Experiment	This Study	Discrepancy
1/3	1/3	35	38.3	+9.6
	2/3	39	38.2	–2.0
	3/3	44	42.9	–2.6
2/3	1/3	34	31.3	–8.1
	2/3	37	34.2	–7.6
	3/3	35	37.5	+7.1
3/3	1/3	32	29.0	–9.3
	2/3	36	36.1	+0.4
	3/3	47	51.0	+8.4

speed, was measured with window width ranging from 1/3 to 3/3 of the wall width. As listed in table2, the discrepancies between the simulations and the published experimental data were less than 9.6%, indicating that the present numerical procedure is adequate and reliable.

4.3 Effect of Fenestration

Table 3 shows MAGE results of Simulation Set 1. As expected, the ventilation rate was mainly affected by inlet layout as opposed to outlet layout. Inlet Layout A produced the smallest values among all four layouts on all floors. Nevertheless, there are interactions among the effects of wind profile and fenestration. The variation of MAGE value caused by the change of inlet layout varied with each floor. On each floor, the largest MAGE value caused by changes in fenestration combinations was approximately 30% more than the smallest one. The increment of MAGE caused by changes in both floor and fenestration combinations can be as large as 96% compared with the smallest one. (Fig. 7)

Based on floor-averaged values of MAGE shown in Table 3, the A-B combination was the smallest among all 16 combinations. The A-B combination was, therefore, adopted for all of the following simulation sets to examine the effect of attachments on building façade.

TABLE 3. MAGE of the breathing zone comparing the 16 combinations of fenestration arrangement. (Unit: s)

		Floor												
		1F				4F				Average				
		Inlet layout				Inlet layout				Inlet layout				
		A	B	C	D	A	B	C	D	A	B	C	D	Average
Outlet layout	A	30.9	37.6	35.1	30.4	40.9	47.6	51.3	40.7	31.8	38.0	38.0	34.2	35.5
	B	27.5	35.3	33.3	33.6	39.9	45.9	50.1	45.8	30.8	37.3	37.4	37.1	35.6
	C	27.6	34.5	33.7	30.8	39.9	44.2	48.3	39.6	31.0	36.6	37.6	32.8	34.5
	D	27.0	35.5	34.7	33.7	41.7	51.4	51.8	44.2	31.7	39.1	38.8	35.8	36.3
Average		28.3	35.7	34.2	32.1	40.6	47.3	50.4	42.6	31.3	37.7	37.9	35.0	

In contrast to the results for MAGE in Simulation Set 1, the air exchange rate was not significantly influenced by air recirculation, as listed in Table 4. Air exchange rate was slightly greater on higher floors, while MAGE increased. Standberg [52] also observed this phenomenon in his experiment. It can be attributed to the difference in deflective angle of incoming wind on each floor. The average value of air exchange rate approximately 22 ACH was much greater than the value suggested by ASHRAE [30] for removing indoor containments from school buildings. Thus, the following analysis emphasized airflow velocity distributions and the MAGE in the student's breathing zone in the analyzed room to examine ventilation efficiency.

FIGURE 7. Maximum and minimum MAGE due to fenestration combination as a function of floor in the breathing zone.

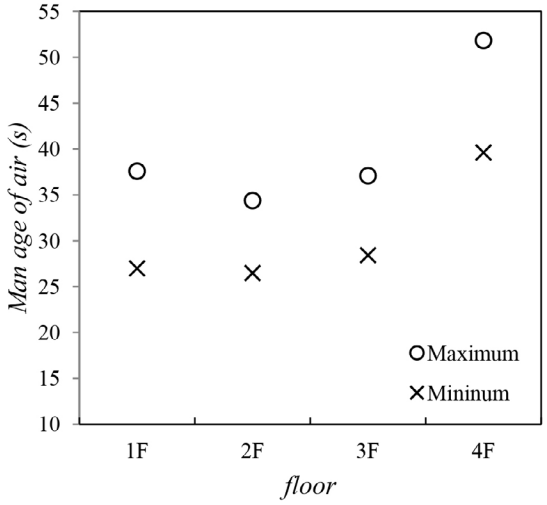

4.4 Complete Model

Simulation Set 2 involved applying the complete model using the A-B combination on each floor. The average value of airflow velocity (Table 5) was stronger on the higher floors which corresponded to a smaller overall average MAGE in the entire room because of the wind profile effect (Fig. 8). The values in the breathing zone, as indicative of air quality for seated students, behaved differently because of an obvious deflection that led airflows away from the breathing zone. MAGE for 4F was approximately 57% more than the value for 1F.

Fig. 9 displays how wind impinged on the windward building façade and flowed into a particular room. The airflow had apparent directionality, governing non-uniform distributions of airflow in the room and was more obvious on higher floors. Hence, hallway and shading devices were used to improve uniformity of air exchange in the following simulation sets.

4.5 Effect of Hallway

Fig. 10 (a) displays the MAGE contour of Simulation Set 3 with hallways and solid handrails on the windward side. Compared with Simulation Set 2, the airflows on 3F and 4F were intercepted by the hallway ceiling and then induced into the rooms. Air flowed across the breathing zone effectively. Fig. 10 (b) shows that higher air velocity on 1F to 4F resulted in 36% to 53% younger MAGE than the model without hallways. Furthermore, the differences in both air velocity and MAGE among floors became relatively small. Hallways on the windward side were effective in directing airflow into the breathing zone, which contributed to increasing the air exchange efficiency.

TABLE 4. Average air exchange rate on each floor. (Unit: 1/hr)

Floor	1F	2F	3F	4F
ACH	21	21	22	24

TABLE 5. Average velocity in the central room of complete model.
(Unit: m/s)

Distance from inlet opening (m)	1F	2F	3F	4F
0	1.07	1.09	1.14	1.29
0.1	0.58	0.59	0.59	0.61
0.6	0.48	0.48	0.49	0.49
1.6	0.41	0.41	0.44	0.41
2.6	0.38	0.39	0.43	0.41
3.6	0.36	0.37	0.41	0.39
4.6	0.33	0.34	0.39	0.38
5.6	0.33	0.33	0.38	0.38
6.6	0.37	0.37	0.41	0.42
7.4	0.43	0.43	0.45	0.48
7.8	0.64	0.64	0.62	0.64
Avg.	0.49	0.49	0.52	0.54

4.6 Effect of Shade Position and Depth

Simulation Set 4 indicated that adding a single shade over an upper window could also effectively decrease MAGE on higher floors, though not as effectively as the much deeper hallways (Figs. 11 and 12). However, the effect on the MAGE varied with difference in shade depth and position among floors. Except for the 0.3-m-deep shade, a deeper shade and higher shade position yielded greater improvements in MAGE. Shades as overhangs more substantially reduced the percentage of MAGE on the higher floors, resulting in greater uniformity among floors. The model with 0.3-m-deep and 0.3-m-upper shades was the only one that resulted in greater (older) MAGE values than that of the model without shades. When 0.6-m and 0.9-m shades were adopted, shades over windows and shades 0.3-m upper than windows yielded a better air exchange rate on the lower floors.

FIGURE 8. MAGE in the central room of the complete model comparing the overall values to the average values at the breathing zone and the values on the central axis of the breathing zone.

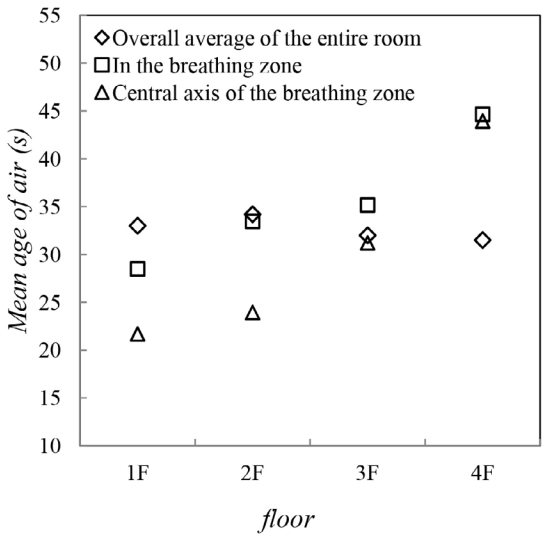

Generally, deeper overhangs were more effective in directing the inclined wind for higher floors. For lower floors, because of flat incoming wind, narrower shades over window were adequate in inducing airflow into the room. The youngest MAGE values obtained when applying horizontal shades for individual floors were not much older than those obtained from the model with hallways.

FIGURE 9. MAGE contour of complete model without attachment.

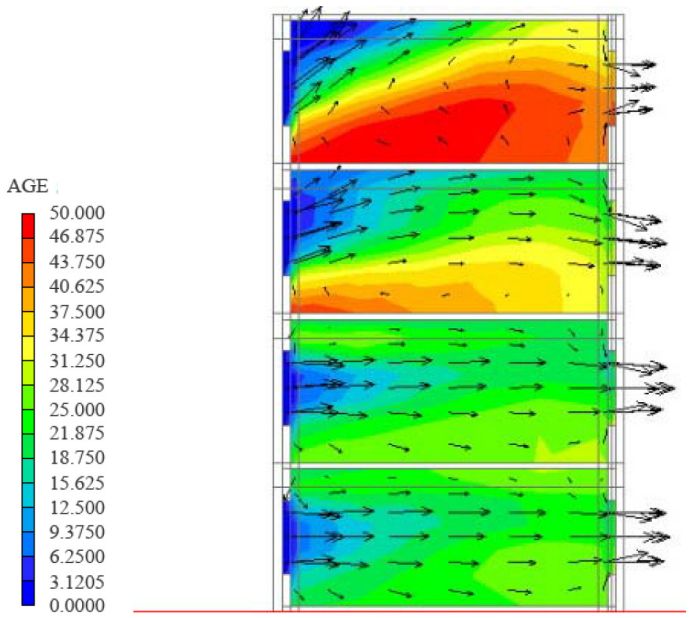

FIGURE 10. (a)–(b) MAGE of complete model with hallway.

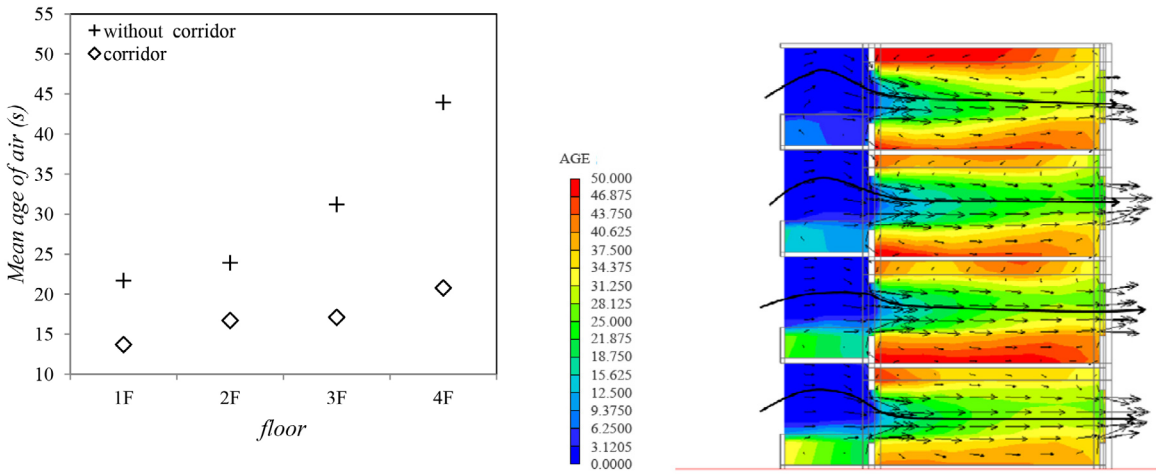

(a) MAGE on each floor

(b) MAGE contour

FIGURE 11. (a)–(c) MAGE of complete model with single shade.

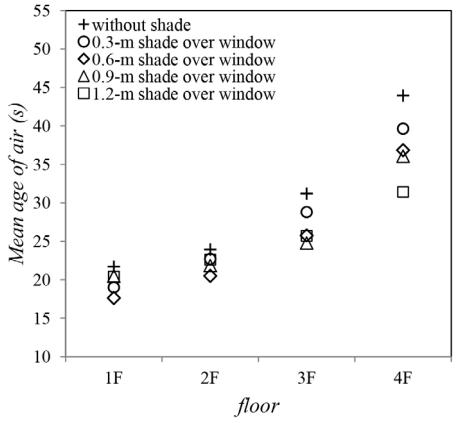

(a) With and without shade over window

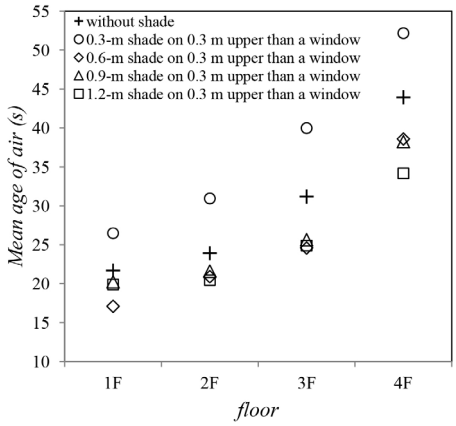

(b) With and without shade on 0.3 m upper than a window

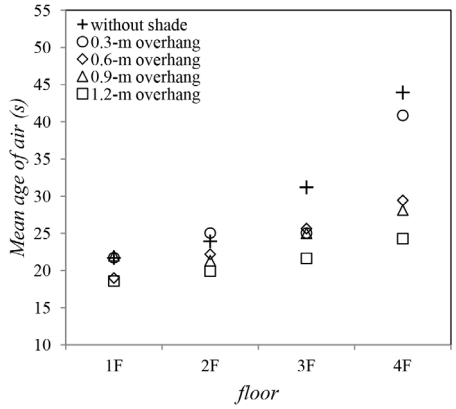

(c) With and without overhang

FIGURE 12. (a)–(c) MAGE contour of complete model with single shade.

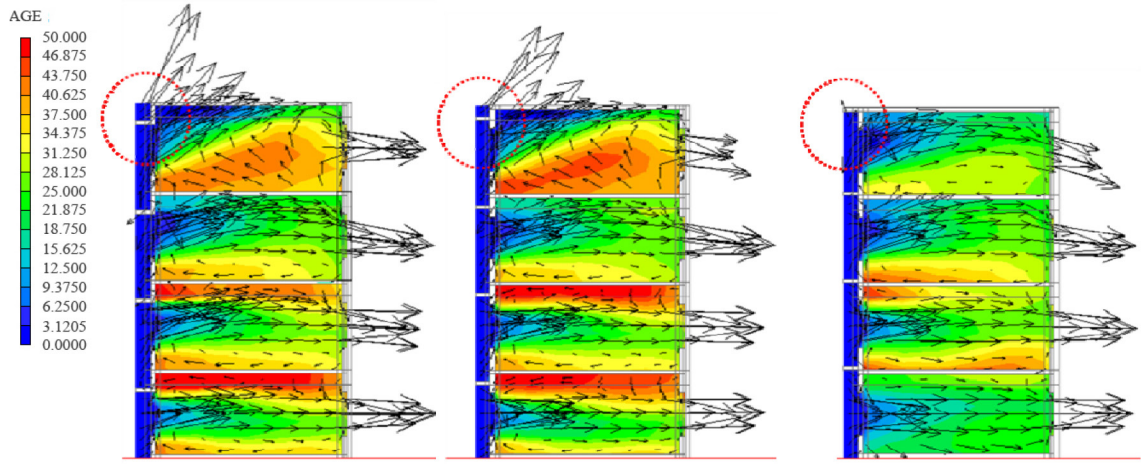

(a) Shade over winow (b) Shade on 0.3-m upper than a window (c) Overhang

4.7 Effect of Slots for Shades over Windows

Fig. 13 indicates that shades with slots weakened the upward wind and resulted in desirable airflow pattern. This result favorably agrees with those from Olgyay's experiment [38]. However, results reveal that superior airflow patterns did not always accompany the lower MAGE in the room. Fig. 13 (a) shows the average MAGE values in different shade lengths and slot depths. Generally the differences on various floors were slight.

FIGURE 13. (a)–(c) Complete model with 1.2-m shade over window.

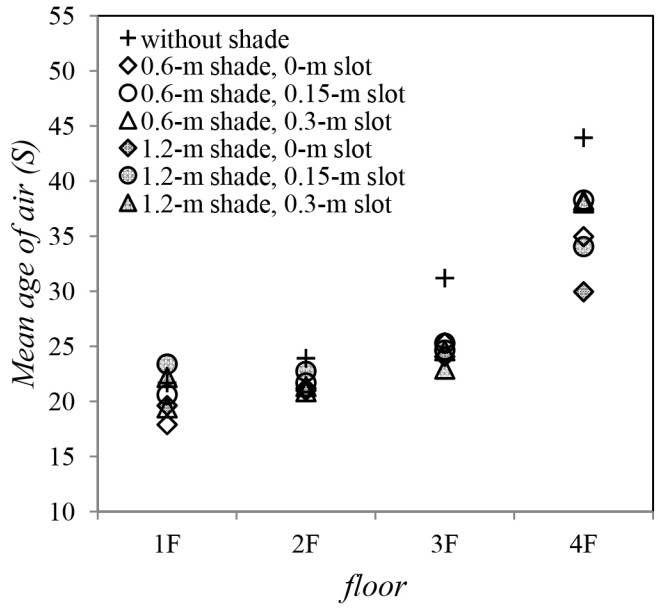

(a) Average MAGE on each floor

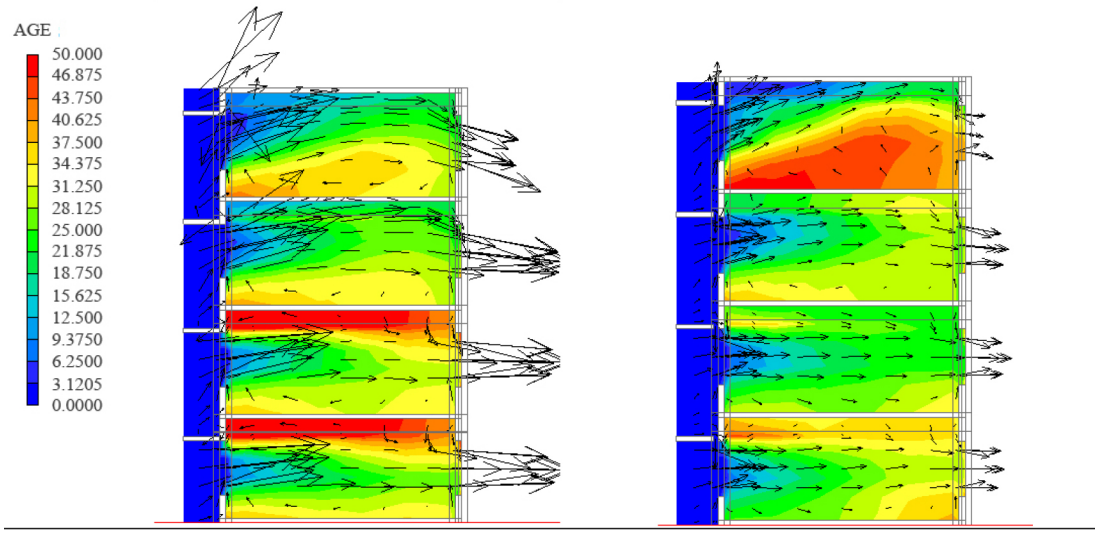

(b) MAGE contour of complete model without a slot

(c) MAGE contour of complete model with a 0.15-m slot

4.8 Effect of Louvers

Fig. 14 shows the wind path that passed through the rooms straightly on lower floors. However, narrower louvers (0.3 m) weakened the velocity on 1F, thus correspondingly resulting in a high MAGE as shown in Fig. 19. On higher floors, deeper louvers significantly contributed to channelling incoming wind through the breathing zone. Using 0.3-m and 0.6-m louvers, MAGE on 4F decreased by approximately 35% and 54%, respectively (Fig. 14 (a)). The results also reveal that incoming wind on 3F, where wind profile effect became stronger, was not adequately deflective to impinge shades and entered the room directly as shown in

FIGURE 14. (a)–(d) Complete model with louver.

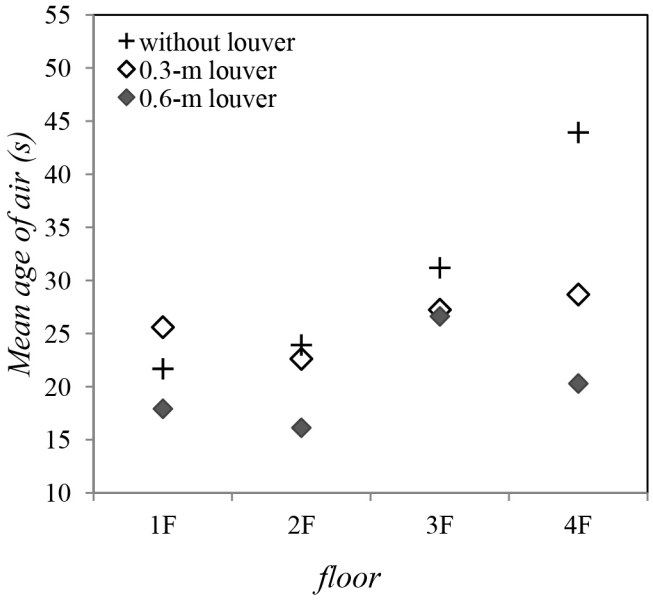

(a) Average MAGE on each floor

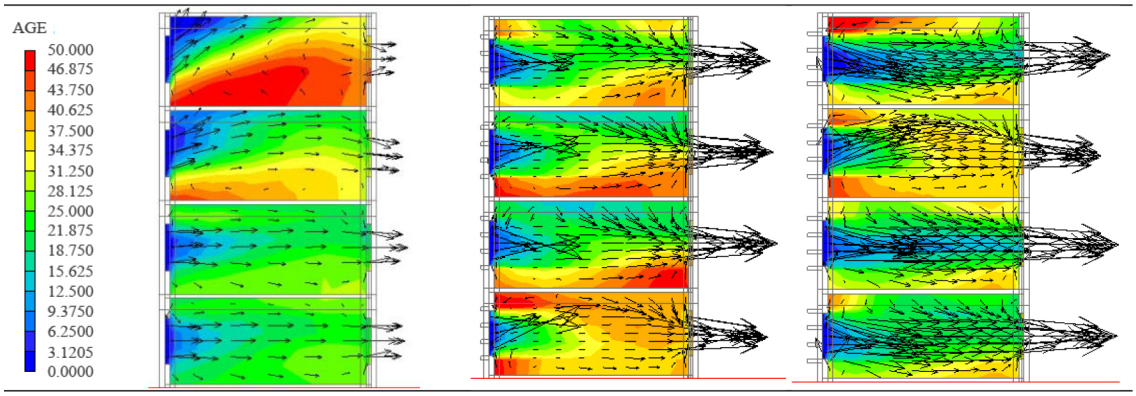

(b) MAGE contour of complete model without louver

(c) MAGE contour of complete model with 0.3-m louver

(d) MAGE contour of complete model with 0.6-m louver

Fig. 15. The incoming wind on 3F caused a higher MAGE than on 4F, despite applying deeper louvers. Therefore, multiple shades used as louver were appropriate for directing airflow on each floor and using deeper shades improved the air exchange rate more effectively.

FIGURE 15. Airflow path of complete model with 1.2m louver on 3F and 4F.

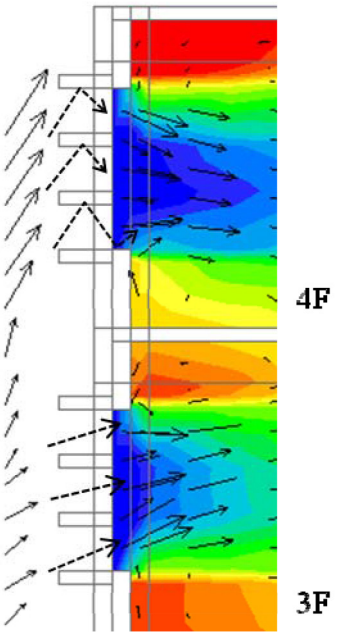

5. CONCLUSION

According to the computational simulation of a typical school building with perpendicular incoming wind from domain inlet that set as 2 m/s at reference height, physical factors such as fenestrations, hallways, and shading devices affect both indoor airflow distributions and MAGE in the breathing zone. The following conclusions can thus be drawn:

a. The wind profile effect causes higher inlet airflow velocities on higher floors, resulting in an inclined angle of incoming wind at inlet toward the ceiling. Deflective incoming wind with a larger velocity on higher floors does not contribute to decreasing MAGE in the breathing zone.
b. Indoor airflow patterns are influenced considerably more by the inlet fenestration layout than by the outlet layout. The optimal fenestration combination in this study resulted in a 30% smaller MAGE than the least favorable combination on the same floor. Differences caused by changes in both floor and fenestration combinations can be as large as 96%.
c. Hallways with 3-m extension of floor can influence the airflow pattern obviously. Incoming wind is directed to centralize toward the breathing zone, thereby improving the ventilation efficiently by reducing MAGE by approximately 53%, which was approximately 23 s in this study. The differences among floors thus become considerably smaller.
d. Deeper single horizontal shades upper than windows are more useful in diverting the inclined airflow toward the breathing zone on higher floors. Using 1.2-m overhangs reduced MAGE by 45% on 4F, only slightly less than the result obtained by introducing hallways. Therefore, depth and position of shades are less critical on the lower floors.
e. Using shades with slot improve airflow patterns. However, this effect barely influences MAGE values.
f. Multiple shades used as louvers can significantly direct incoming wind, and deeper shades apparently decrease MAGE in the breathing zone more effectively. However, the improvement is not as effective on 3F, where the angle of the incoming wind is slight.0.6-m louvers decrease MAGE by 52% on 4F.

REFERENCE

1. H.B. Awbi, Design considerations for naturally ventilated buildings, Renew. Energy. 1994; 5:1081–2090.
2. I.A. Raja, J.F. Nicol, K.J. McCartney, Natural ventilated buildings: use of controls for changing indoor climate, Renew. Energy. 1998; 15:191–934.
3. N.M. Guirguis, G.B. Hanna, M.F. Kotkata, I.A. Gad, An investigation of building/wind interaction, Renew. Energy. 1998; 15: 383–386.
4. S. Kato, S. Murakami, Takahashi, T. Gyobu, Chained analysis of wind tunnel test and CFD on cross ventilation of large-scale market building, J. Wind Eng. Ind. Aerodyn. 1997; 67–68:573–587.
5. V. Straaten, Thermal Performance of buildings, Elsevier, Amsterdam, 1967.
6. B.J. Vickery, C. Karakatsanis, External wind pressure distributions an induced internal ventilation flow in low-rise industrial and domestic structures, ASHARE Trans. 1982; 93:2198–2213.
7. G.C. Graca, Q. Chen, L.R. Glicksman, L.K. Norford, Simulation of wind-driven ventilation cooling systems for an apartment building in Beijing and Shanghai, Energy Build. 2002; 34:1–11.
8. J.Seifert, Y. Li, J. Axley, M. Rösler, Calculation of wind-driven cross ventilation in buildings with large openings, J. Wind Eng. Ind. Aerodyn. 2006; 94:925–947.
9. Z. Zhai, S.D. Hamilton, J. Huang, C. Allocca, N. Kobayashi, Q. Chen, Integration of indoor and outdoor airflow study for natural ventilation design using CFD, in: Proceeding 21st AIVC Annual Conference: Innovations in Ventilation Technology, The Hague, 2000.
10. S.S. Ayad, Computational study of natural ventilation, J. Wind Eng. Ind. Aerodyn. 1999; 82:49–68.
11. K. Visagavel, P.S.S. Srinivasan, Analysis of single side ventilated and cross ventilated rooms by varying the width of the window opening using CFD, Sol. Energy. 2009; 83:2–5.
12. E. Prianto, P. Depecker, Optimization of architectural design elements in tropical humid region with thermal comfort approach. Energy Build. 2003; 35:273–280.
13. W.H Chiang, C.J. Wu, K.Y. Weng, L.D. Yang, The effects of façade design on cross ventilation for Taiwanese classroom. ASHRAE Trans. 2005; 111:333– 339.
14. A.A Argiriou, C.A. Balaras, S.P. Lykoudis, Single-sided ventilation of buildings through shaded large openings, Energy. 2002; 27:93–115.
15. Q. Chen, Ventilation performance prediction for buildings: A method overview and recent applications, Build. Environ. 2009; 44:848–858.
16. J.J. Kim, J.J. Baik, A numerical study of the effects of ambient wind direction on flow and dispersion in urban wind direction on flow and dispersion in urban street canyons using the RNG K-ε turbulence model, Atmos. Environ. 2005; 38:3039–3048.
17. A. Mochida, I.Y.F. Lun, Prediction of wind environment and thermal comfort at pedestrian level in urban area, J. Wind Eng. Ind. Aerodyn. 2008; 96:1498–1527.
18. J. Hang, M. Sandberg, Y. Li, Age of air and air exchange efficiency in idealized city models, Build. Environ. 2009; 44:1714–1723.
19. G. Evola, V. Popov, Computational analysis of wind driven natural ventilation in buildings, Energy Build. 2006; 38:491–501.
20. J.D. Posner, C.R. Buchanan, D.D. Rankin, Measurement and prediction of indoor airflow in a model room, Energy Build. 2003; 35:515–526.
21. T. Karimipanah, H.B. Awbi, M. Standberg, C. Blomqvist, Investigation of air quality, comfort parameters and effectiveness for two floor-level air supply systems in classrooms, Build. Environ. 2007; 42:547–655.
22. H.B. Awbi, Energy efficient room air distribution. Renew. Energy 1998; 15:293–299.
23. S.I. Tanabe, K. Kobayashi, J. Nakano, Y. Ozeki, M. Konishi, Evaluation of thermal comfort using combined multi-node thermoregulation (65MN) and radiation models and computational fluid dynamics (CFD), Energy Build. 2002; 34:637–646.
24. J.S. Russo, T.Q. Dang, H.E. Khalifa, Computational analysis of reduced-mixing personal ventilation jets, Build. Environ. 2009; 44:1559–1567.
25. S.H. Ho, L. Rosario, M.M. Rahman, Three-dimensional analysis for hospital operating room thermal comfort and contaminant removal, Appl. Therm. Eng. 2009; 29:2080–2092.

26. Y. Jiang, D. Alexander, H. Jenkins, R. Arthur, Q. Chen, Natural ventilation in buildings: measurement in a wind tunnel and numerical simulation with large-eddy simulation, J. Wind Eng. Ind. Aerodyn. 2003; 91:331–353.
27. C.C. Hsu, T.K. Huang, The plane of module size for dwelling house and school building. Architecture and Building Research Institute, Ministry of the Interior, Taipei, 1991.
28. V. Olgyay, Design with climate, Van nostrand reinhold, New York, 1992.
29. ASHRAE, ASHRAE Handbook fundamentals, ASHRAE, Atlanta, 2005.
30. ASHRAE, ASHRAE Standard 62-1989: Ventilation for acceptable indoor air quality, Atlanta, 1989
31. ASHRAE, ASHRAE Handbook, ASHRAE, Atlanta, 2009.
32. V. Chanteloup, P.S. Mirade, Computational fluid dynamics modeling of mean age of air distribution in forced-ventilation food plants, J. Food Eng. 2009; 90:90–103.
33. X. Li, D. Li, X. Yang, J. Yang, Total air age: an extension of the air age concept. Build. Environ. 2003; 38:1263–1269.
34. D. Etheridge, M. Sandberg, Building ventilation theory and measurement, John wiley & sons, Chichester, 1996.
35. G. Gan, Effective depth of fresh air distribution in rooms with single-sided natural ventilation, Energy Build. 2000; 31:65–73.
36. H.B Awbi. Ventilation of buildings, 2nd edition, Spon Press, 2003.
37. J. Franke, A. Hellsten, H. Schlünzen, B. Carissimo, COST Action 732: Best practice guideline for the CFD simulation of flows in the urban environment, Cost, Hamburg, 2007.
38. Q. Chen, Prediction of room air motion by Reynolds-stress models, Build. Environ. 1996; 31:233–244.
39. Q. Chen, Comparison of different k-ε models for indoor airflow computations, Numer Heat Tranf. B-Fundam. 1995; 28:353–369.
40. F. Allard, Natural ventilation in buildings: a design handbook, second ed., James & James, London, 2002.
41. PHEONICS 2009 (software package), FLAIR User's Guide, CHAM Ltd., London, 2009.
42. Y. Tominaga, A. Mochida, R. Yoshie, H. Ktaoka, T. Nozu, M. Yoshikawa, T. Shirasawa, AIJ guidelines for practical applications of CFD to pedestrian wind environment around buildings. J Wind Eng Ind Aerod. 2008; 96: 1749–1761.
43. P.J Richards, R.P. Hoxey, Appropriate boundary conditions for computational wind engineering models using the k-ε turbulence model, J Wind Eng Ind Aerod.1993; 46 & 47: 145–153.
44. P.J Richards, and S.E. Norris, Appropriate boundary conditions for computational wind engineering models revisited, J Wind Eng Ind Aerod.2011; 99: 257–266.
45. G. Gan, H.B. Awbi, Numerical simulation of the indoor environment. Build. Environ. 1994; 29: 449–459.
46. B. Givoni. Man, Climate and Architecture, Van nostrand reinhold company, 1981.
47. M. Melaragno, Wind in Architectural and environmental design. Van Nostrand Reinhold, 1982.
48. G. Z. Brown and Mark Dekay, Sun, wind & light: architectural design strategies, 2nd edtion. John wiley & sons, inc, 2001.
49. A. M. Omer, Constructions, applications and the environment of greenhouses, Afr. J. Biotechnol. , 2009; 8(25): 7205–7277.
50. J. Kindangen, G. Krauss, P. Depecker,Effects of roof shapes on wind-induced air motion inside buildings, Build. Environ. 1997; 32(1):1–11.
51. Kolawole Ajibola, Ventilation of spaces in a warm, humid climate—Case study of some housing types, Renew. Energy 1997; 10(1):61–70.
52. M. Sandberg, What is ventilation efficiency? Build. Environ. 1981; 16: 123–135.

APPENDIX 1: NOMENCLATURE

C_μ	Turbulent model constant
H	building height
k	turbulence kinetic energy
L	building length
MAGE	mean age of air
n	air change rate per hour
Q	volumetric airflow rate
U	total velocity at Z height from ground
U_r	velocity at reference height
U^*	total friction velocity
u_i	velocity components in x, y, z direction
V	interior volume of a space
W	building width
Z_o	effective roughness height of the ground terrain
Z_r	reference height

Greek Symbols

α	power-low exponent
ε	dissipation rate of turbulence kinetic energy
ε_α	air exchange efficiency
κ	von Karman's constant
σ	laminar Schmidt number of air
σ_κ	turbulence model constant
σ_ε	turbulence model constant
$\sigma_{\varepsilon 2}$	turbulence model constant
$\sigma_{\bar{\tau}}$	turbulent Schmidt number for the age of air
$\bar{\tau}$	internal mean age of air
υ	laminar kinematic viscosity
υ_t	turbulent kinematic viscosity